Chapter 6

RF Bulk Acoustic Wave Resonators and Filters

H.P. Loebl [a], C. Metzmacher [a], R.F. Milsom [b], P. Lok [c], A. Tuinhout [c]
[a] *Philips Research Laboratories, Weisshausstr.2, D-52066 Aachen, Germany*
[b] *Philips Research Laboratories, Cross Oak Lane; Redhill; Surrey, RH1 5HA, UK*
[c] *Philips Semiconductors, BL RF products, Gerstweg2, NL-6534 AE Nijmegen, The Netherlands*

Small sized, highly selective solidly mounted bulk acoustic wave (BAW) band pass filters are of great interest for mobile and wireless systems operating in the frequency range of 0.8 GHz up to more than 10 GHz. Applications for BAW filters include front-end filters for USPCS, UMTS, GSM, bluetooth and other standards. BAW filters can be fabricated on silicon or glass wafers using standard semiconductor production techniques. On-wafer packaging techniques allow to fabricate small, flip chip mountable BAW filter devices suited for System in Package (SiP) solutions.

The chapter explains the how BAW filters work, compares their performance with competing filter technologies (e.g. surface acoustic wave filters), describes the technique Philips uses to realize BAW filters and reviews briefly alternative technical approaches. BAW filters are based on electro-acoustic high Q resonators, which exploit the thickness extensional mode of a thin, highly oriented, piezoelectric AlN or ZnO film. One section of the chapter is devoted to the growth of piezoelectric AlN films, which have to be grown with the polar c-axis, oriented perpendicular to the substrate. It is shown that both the sputter deposition process and using a textured, well oriented electrode support excellent c-axis oriented growth of the AlN films. An example is the growth of AlN (0002) on Pt (111) oriented electrodes where we find an epitaxial relation. The growth mechanism of AlN films, which grow highly oriented as well on amorphous and smooth surfaces like SiO2 and the thickness dependence of their orientation is discussed. We show that AlN (0002) orientation is directly correlated with the electromechanical coupling coefficient k_t of the films and therefore with the filter bandwidth.

The following section describes the modeling techniques we use to describe the filter and resonator response. A combination of a 1 dimensional analytical electro-acoustic model together with an electromagnetic model reveals optimal agreement between measurement and simulation. It is shown that the small details of the resonator

and filter curves can be used to extract relevant material data. Embedding the electro-acoustic model into a commercial circuit simulator offers an excellent method for the designer to predict filter performance. The limits of this 1-D model are discussed briefly referring the reader to a more rigorous 2-D treatment of BAW resonators, which would allow to explain major acoustic loss mechanisms. Finally a few examples of filters operating in the range between 2 and 8 GHz are shown.

1. Introduction

Filtering of signals, which are closely separated in the frequency domain, is a key function in mobile radio front-ends (see Figure 1). The performance requirement means that this function must be implemented in a passive technology. 3G mobile standards like UMTS, where transmission and reception of signals is done simultaneously require narrow band filters (duplexers), which have flat pass- band with steep skirts and high out-of-band rejection. For that reason thin-film bulk acoustic wave (BAW) resonators, BAW ladder and lattice filters and acoustically coupled BAW filters have been studied intensively over the past 20 years for RF applications in the frequency range of 800MHz to 12 GHz [1–6, 14, 16, 20].

The use of BAW filters for radio front ends of mobile phones, in particular, has attracted a lot of interest, since surface acoustic wave (SAW) filters, which are well established at frequencies up to approx. 2GHz, have considerable drawbacks at higher frequencies: sub-micron lithography, dedicated small wafer-size expensive non silicon substrates such as $LiNbO_3$ or $LiTaO_3$, and poor power handling characteristics [27]. Ceramic resonator filters, which are also used in this frequency range, on the other hand, suffer from their relatively large size and low integration potential. BAW filters are remarkably small in size, can be processed on silicon or glass using standard silicon integration techniques. Furthermore, they can be designed with a low temperature coefficient of frequency (TCF), which is a very important requirement for accurate narrow band filters [24, 25]. This all makes BAW filters very attractive for today's semiconductor industry. The essential building blocks of these BAW filters are small sized BAW resonators (see Figure 2), which, in the technology of interest here, exploit the thickness extensional vibration mode of a thin piezoelectric film.

The resonance frequency f_r is determined approximately by the thickness t of the piezoelectric film:

$$f_r = v_l/\lambda \approx v_l/2t \tag{1.1}$$

where v_l is the longitudinal velocity of sound in the normal direction in the piezoelectric layer, t is the thickness of the piezoelectric film, and λ is the acoustic wavelength. In

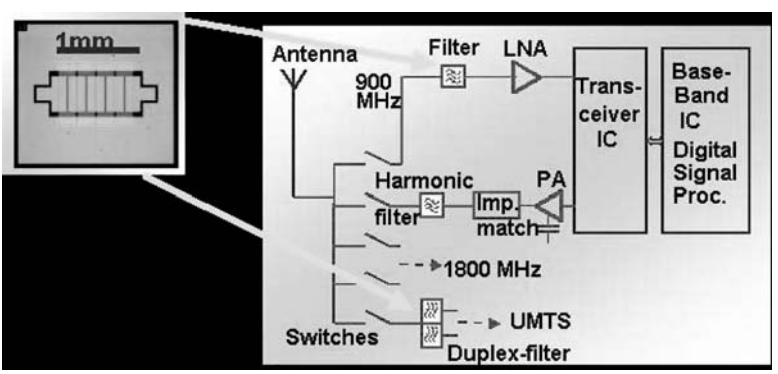

Fig. 1. Architecture of a mobile phone front end. Filters are required in e.g. GSM (900 MHz, 1800 MHz) and UMTS bands. Left: example of a die with a 4-section BAW ladder filter.

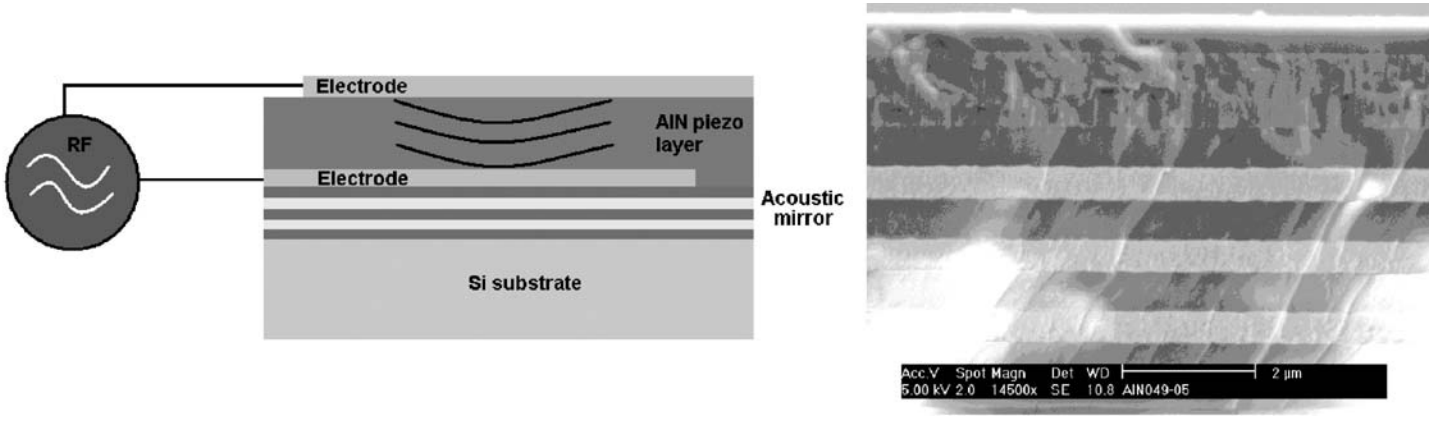

Fig. 2. Bulk acoustic wave resonator. Left: schematic showing acoustic Bragg reflector (acoustic mirror), electrodes, and piezoelectric layer; right: SEM cross-section of BAW resonator.

a real resonator device, of course, the frequency f_r is different from eq. (1.1), since the acoustic properties of all other layers influence the resonator performance e.g. by the mass-loading effect of the resonator's electrodes. Despite the fact that equation (1.1) is only a crude approximation one can draw two important conclusions:

1. Since the velocity of sound is typically in the range between 3000–11000 m/s for most materials, we need a thickness of the piezo layer in the order of a micrometer.
2. The frequency of a resonator and thus the center frequency of a filter are mainly determined by the thickness t of the piezo layer. This poses also a strong challenge on the accuracy of thin film deposition. Despite the fact that the idea for high frequency BAW filters is already quite old, only the large improvements in the field of sputter deposition techniques over the past few years has made thin-film BAW resonators and filters technologically feasible.

For low loss BAW filters the acoustic energy has to be confined within the resonator. This is done by using an acoustic reflector, which reflects the energy back into the resonator. One implementation of such a reflector is realized using etching techniques adapted from micro electro mechanical systems (MEMS) technology. Here the thin film BAW resonator (TFBAR) is formed on a thin membrane of Si, SiO_2, or Si_3N_4. Since the acoustic impedance of air is negligible compared to the acoustic impedance of solids, almost all the energy is reflected back from the resonator/air interface. The TFBAR technology is applied industrially for PCS band duplex filters [15]. Another approach is the solidly mounted BAW resonator (SBAR). This reflector technique utilizes so-called Bragg mirrors consisting of a stack of thin layers of materials with alternate high and low acoustic impedance (acoustic impedance $= \rho \times v_1$, where ρ is the density). Various material combinations exist for such acoustic interference coatings e.g. SiO_2/AlN [1, 2, 4, 25], SiO_2/W [20], SiO_2/metal-oxides [29]. Depending on the difference in acoustic impedance an effective reflector typically requires up to 5 pairs of layers. Figure 2 below shows a typical BAW resonator. The bottom electrode is made of a high conductivity material such as Al, Mo, W, or Pt. For the piezoelectric layer either AlN [1, 2, 4, 14, 17, 18], or ZnO [20, 22] is commonly used. Alternative materials including ferroelectrics are presently under discussion [7, 8, 9, 21]. Both AlN and ZnO have the hexagonal wurtzite type structure, i.e. in order to get a working device, the material has to be grown with the polar c-axis perpendicular to the substrate surface. Additionally the polarity may not change across the BAW resonator. The top electrode is again made of a high conductivity material.

In Figure 3 one can see the electrical impedance of a BAW resonator with its two characteristic frequencies. At the resonance frequency f_r the electrical impedance |Z| is very small (electrical field parallel to polarization, high current flowing) whereas at the anti-resonance frequency fa |Z| is very large (electrical field anti-parallel to polarization, no current flowing). As mentioned above, filters are made by combining several resonators. Figure 3 shows a simple one-section ladder filter comprising a series and a parallel resonator (s,p). The parallel resonator p is shifted in frequency with respect to the series resonator s. When the resonance frequency f_{r_s} of the series resonator equals the anti-resonance frequency f_{a_p} of the parallel resonator, maximum signal is transmitted from input to output of the device. At the anti-resonance frequency f_{a_s} of the series resonator filter transmission is blocked, and at the resonance frequency

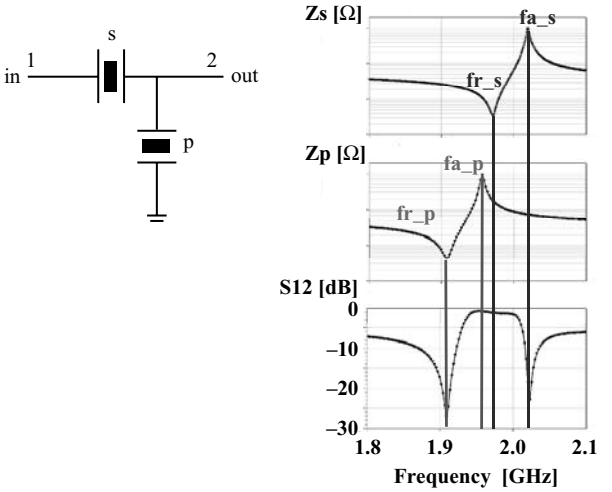

Fig. 3. Single section BAW filter consisting of one series and one parallel resonator. Right: Electrical impedance of series and parallel resonator. The bottom curve shows the transmitted signal S_{21} revealing a band-pass filter characteristic.

of the parallel resonator f_{r_p} the filter input is connected to ground, so that the BAW filter also blocks signal transmission at this frequency. This results in the band-pass filter characteristic S21 shown in figure 3. The out-of-band rejection is typically 6 dB for a single filter section. The bandwidth of the filter is determined by the separation of f_r and f_a and is therefore proportional to the square of the electromechanical coupling coefficient k_t^2 (see eq. 1.2). Pulling the resonance frequency of the series resonator f_{r_s} and the anti-resonance frequency of the parallel resonator f_{a_p} apart, as shown in Figure 3, increases the bandwidth slightly. The dip in the center of the pass-band (see Figure 3 and Figure 12) can be recovered partially by adding small inductors at the filter ports.

$$k_t^2 = \frac{\pi^2}{4}\left(\frac{fa - fr}{fa}\right) \tag{1.2}$$

k_t^2 is approximately 6.25%–7% for AlN and 8.5% for ZnO. This appears to be sufficient for many mobile and wireless filter applications. Certainly ZnO would be preferable because it could offer a wider bandwidth. However, we have to consider the temperature dependence of the elastic, piezoelectric and dielectric constants and thermal expansion coefficient, which together result in a temperature coefficient of the resonance frequency TCF. For AlN and ZnO reported values are −25 ppm/K and −60 ppm/K respectively [23]. For the temperature dependence of the whole device the other layers (mass-loading layer, electrodes) also have to be considered. Reported values of TCF are −19 to −21 ppm/K for AlN SBAR filters, 0 ppm/K for compensated AlN TFBAR resonators [25], and −31 ppm/K for ZnO based SBAR filters [20]. The higher TCF for ZnO compared to AlN appears to be a drawback.

2. Experimental

In the following we describe typical experimental techniques for the fabrication of solidly mounted SBAR devices. Resonators and filters were fabricated on 6" silicon wafers and for comparison on glass wafers [7, 8, 9, 11]. We commonly used an acoustic reflector comprising λ/4 layers of high and low acoustic impedance materials. The thickness of the reflector layers was controlled optically. Electrode materials were Al, Mo and Pt. The piezoelectric layer was c-axis oriented AlN, which was deposited by pulsed reactive DC magnetron sputtering in a Unaxis CL200-cluster tool. The base pressure was in the low 10^{-8} mbar range. A pulse frequency of 20–100 kHz was used to avoid arcing. Chuck temperature was varied between 300 °C and 500 °C, and a RF substrate bias was applied to control stress and texture of the AlN films. The quality of the AlN films was routinely checked by X-ray diffraction $\theta/2\theta$ scans (Philips Fine Focus PW2213/20) and by measuring the full width at half maximum (FWHM) of the rocking curve of the AlN 0002 peak. The quality of the AlN films was excellent. A FWHM of 1.2–1.5° was achieved on Si substrates; approximately 1.5° was achieved on Pt electrodes. The AlN properties varied only slightly with the deposition conditions [9, 11]. Resonators and filters were measured electrically (one and two port measurements) on wafer level using wafer microprobes. The measurements were done with an R&S Vector Network-Analyzer in a frequency range between 10 MHz and 20 GHz with increased resolution in the vicinity of the resonance.

3. Microstructure of AlN

AlN and also ZnO have a hexagonal (6mm) wurtzite type structure (see Figure 4). When an electric field is applied along the polar c-axis, atoms and consequently the center of charge are displaced and the unit cell is strained. This effect represents the so-called inverse piezoelectric effect and is exploited in BAW resonators and filters. By applying an alternating RF field along the c-axis the BAW resonator is excited in its thickness extensional mode. Figure 4 reveals that the AlN film has to be grown c-axis

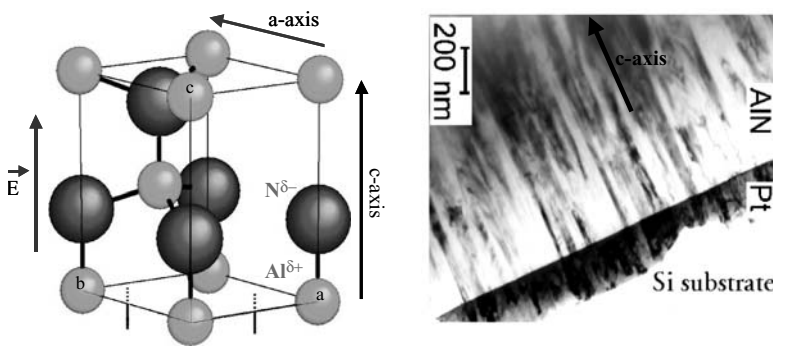

Fig. 4. Left: Schematic view of an AlN unit cell showing polar character. Right: TEM cross-section of a c-axis oriented polycrystalline AlN film on a Pt (111) electrode.

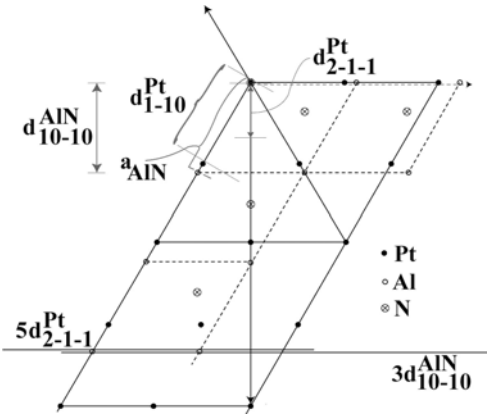

Fig. 5. Epitaxial relationship of AlN(0002) on Pt(111) in plan view, i.e. along AlN[0001] and Pt[111] direction. Dashed lines: unit cell of AlN, solid lines: 'hexagonal cell' of Pt.

oriented and that the a-axis is hereby randomly oriented in the substrate plane. The AlN film is a columnar grown and textured poly-crystal with a grain size (column width) of typically 35 nm.

C-axis oriented growth of AlN appears to be the naturally supported orientation, because it comes along with a with the hexagonal-closed packed (hcp) arrangement of N and Al atoms in the sequence of a double layer stacking according to . . . AA'BB'AA'. . . . As long the growth of the AlN film is not disturbed, c-axis orientation will be the preferred orientation. Furthermore, the use of polycrystalline, textured electrodes may support c-axis oriented growth [8, 19]. In Figure 4 a TEM bright field cross-section of a Pt electrode with (111) orientation is shown. The TEM image indicates that the AlN growth occurs quasi-epitaxially and the Pt grain size and AlN grain-size match quite distinctly. Quasi-epitaxy can be deduced from the degree of texture of both AlN and Pt electrode and has been proved by selected area electron diffraction and micro diffraction in TEM in addition to macroscopic XRD. Indeed, an epitaxial orientational relationship exists (see Figure 5) which describes the growth of (0002) oriented AlN on Pt (111) geometrically according to the matching condition (3.1):

$$5 \cdot {d_{2\bar{1}\bar{1}}}^{Pt} = 3 \cdot {d_{10\bar{1}0}}^{AlN} \tag{3.1}$$

Another important aspect of the growth of AlN is the thickness dependence of the AlN texture. As shown in Figure 6, AlN was grown in subsequent runs, each run depositing a AlN film thickness of approximately 1 μm. After each deposition an XRD rocking curve of the AlN0002 peak was measured. It can be seen that the rocking curve FWHM width of the (0002) peak gets smaller from run to run and that the net intensity of the 0002 peak becomes larger. The AlN c-axis orientation improves with thickness, if the growth is not disturbed. The TEM image reveals, that the orientation of the AlN crystallites in the beginning of the growth is misaligned with respect to perfect (0002) orientation. Since the (0001) oriented grains grow faster at the expense of the misaligned grains, we find eventually after a few 100 nm almost perfect c-axis

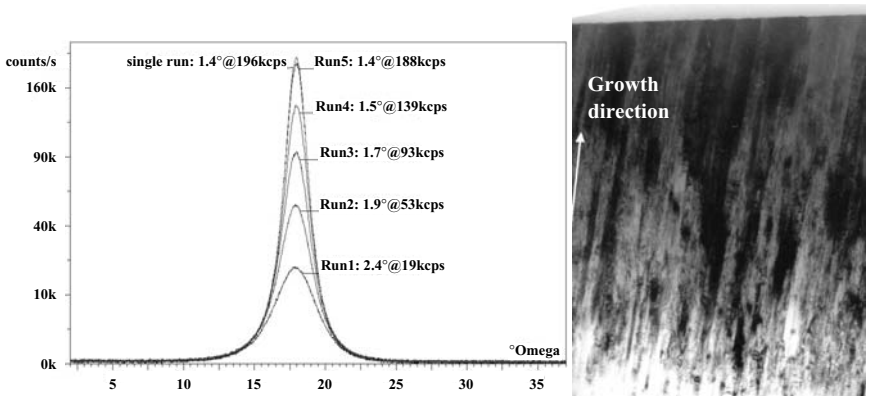

Fig. 6. Top left: XRD rocking curves of the AlN0002 peak of AlN films with different thickness. C-axis orientation improves from run to run. Right: TEM cross-section of thick AlN layer showing improvement of c-axis texture with thickness micro-structurally.

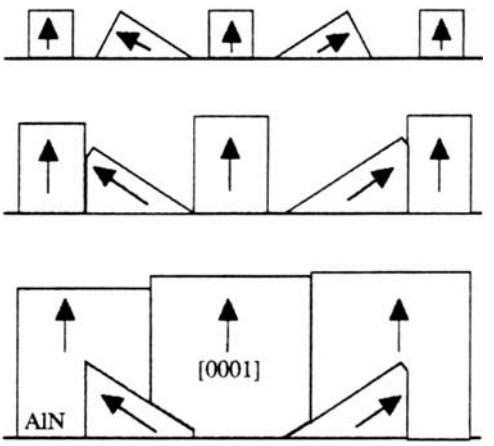

Fig. 7. Schematic depiction nucleation and growth mechanism of AlN according to ref. [26].

orientation of the AlN grains. The AlN growth mechanism is schematically depicted in Figure 7.

The dependence of the experimentally determined coupling coefficient k_t on the rocking curve FWHM width of AlN0002 peak is shown in Figure 8 [11]. Films with poor c-axis orientation have significant lower values of the coupling coefficient k_t with consequently reduced filter bandwidth. As can be seen in Figure 9, the sputter deposition process results in good oriented films both on SiO_2 and on Pt(111) substrate surfaces. The dependence of the AlN orientation on the sputter conditions is only small. Generally higher substrate temperature and moderate RF bias applied to the substrate support c-axis orientation most probably due the increased mobility of the sputtered N and Al ad-atoms at the substrate surface. In ref. [17,18,19] it was shown, that the

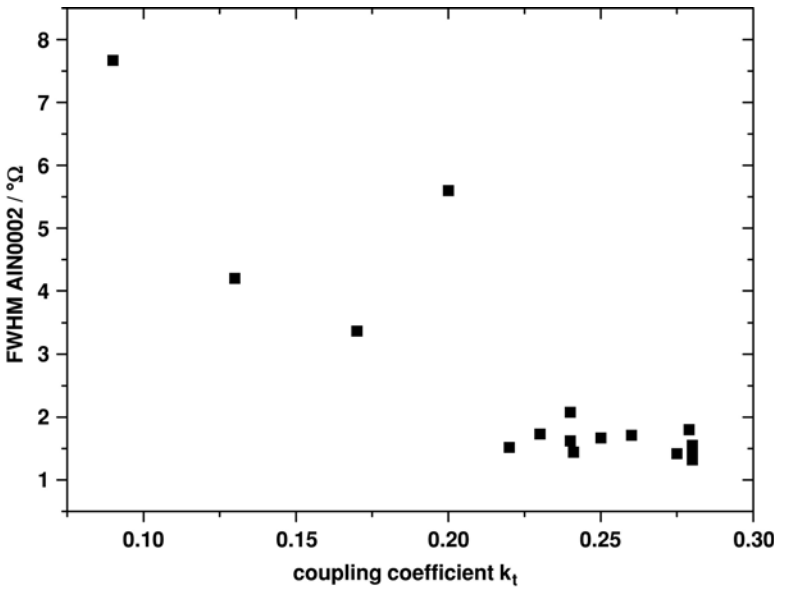

Fig. 8. Dependence of coupling coefficient k_t on the rocking curve FWHM of the AlN0002 peak. Poorly oriented films show low coefficient k_t.

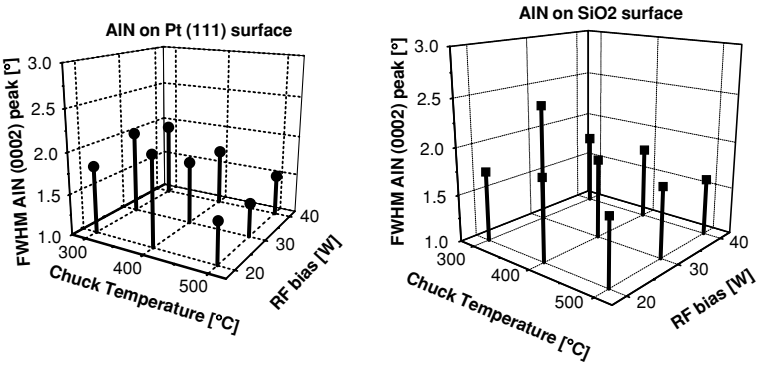

Fig. 9. Dependence of AlN c-axis orientation on process conditions. FWHM width of AlN(0002) peak depends only weakly from deposition conditions. Left: AlN on Pt(111) surface, right: AlN on thermal SiO_2 surface.

piezoelectric constant d_{33} and thus k_{33} or k_t is influenced by the bias applied to the substrate.

4. Simulation

In order to meet the demanding specifications typical in BAW filter applications it is important to optimize all aspects of the resonator and filter performance, and therefore to consider both acoustic and electromagnetic (EM) contributions to the

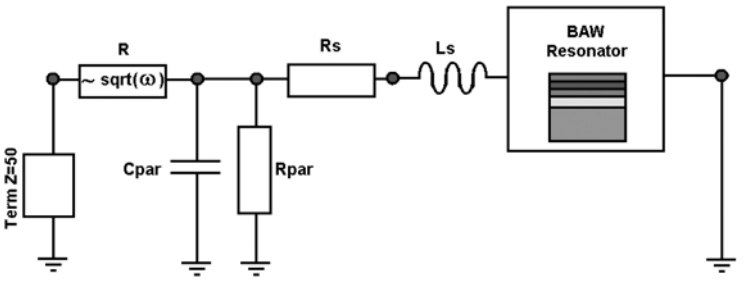

Fig. 10. Simulation of a BAW resonator: The electro acoustic 1-D resonator model described by the symbol right is imported in a commercial circuit simulator. The EM contributions are simulated as lumped elements.

filter behaviour. In particular, many mechanisms contribute to pass-band insertion loss. These include conductor loss, dielectric loss in the piezoelectric layer, substrate loss, electrical mismatch loss, acoustic loss in the materials and several additional acoustic loss mechanisms. On the other hand, rejection in the stop-band is typically limited by electrical (electromagnetic) effects. To help address related design issues, a method has been developed for simulating the different physical effects in a unified model. Computational efficiency is important in the design cycle, therefore a 1D electro-acoustic solution broadly equivalent to the model of Nowotny and Benes [10] is used to model the BAW resonators, while lumped-element equivalent-circuit models are used for modeling the EM part of the problem. In the first method, appropriate for modeling parasitics due to filter layout, lumped component values are extracted automatically from 2.5D EM simulation using the method described in [13]. The second method, appropriate for modeling single resonators, uses the simpler procedure: lumped elements describing parasitics are added either in series or parallel with the electro-acoustic model (see Figure 10).

The acoustic material loss of the resonator is described by the material quality factor Q_m of each layer, which we introduce into the model through an imaginary component of the longitudinal sound velocity. Parasitic components due to interconnects are introduced into the model to match the measurements as closely as possible. Series resistance R and inductance L of the electrodes are added to the resonator model as lumped elements in the circuit simulator. Additionally a term proportional to $\sqrt{\omega}$ (square root of angular frequency) is included in the resistance. This approximately accounts for the RF-dependent redistribution of current in the conductors. A parasitic capacitor and resistor to ground model the stray electric field and associated loss in the Si substrate. Dielectric loss is characterized by introducing by an imaginary part into the dielectric constant of AlN.

We introduce additional loss (to account for otherwise unexplained measured loss) through an imaginary part of k_t. This is seen to improve the agreement with measurement. Alternatively it has been proposed to introduce an additional resistor in series with the static capacitance of the resonator [12]. Neither way of describing this additional loss mechanism seems to be justified on physical grounds. We suspect that the predominant additional loss mechanism may actually be acoustic radiation away from

the resonator associated with imperfect energy trapping. A more rigorous treatment of this effect would require 2-D or even full 3-D modeling of the BAW resonators [28, 29].

5. Resonator and Filter Performance

By means of an acoustic Bragg reflector high Q factor resonators can be made. Figure 11 shows the electrical impedance Z and admittance Y of a series resonator (two identical resonators connected in series via the bottom electrode) for 1.95 GHz. The AlN thickness in this resonator was approx. 1900 nm; the resonator area was $268 \times 268\ \mu m^2$. For the bottom electrode we used (111) oriented Platinum, for the top electrode Aluminium was used. The acoustic reflector consisted of alternating $\lambda/4$ layers of SiO_2 and a metal oxide with low and high acoustic impedance respectively. The quality factor Q_z at the anti-resonance was approximately 750, the quality factor at the resonance Q_y was approx. 1014. The simulation was done using the combined 1-D electro-acoustic model (Nowotny & Benes theory) and the simpler of the two electromagnetic models described above. The acoustic material loss of the resonator is described by the material quality factor Q_m of each layer, which we introduced into the model through an imaginary component of the longitudinal velocity of sound v_l (see above). Parasitic components due to interconnections were introduced into the model to match the measurements accurately. A more fundamental treatment of parasitics based on an electromagnetic simulation of the filter layout is described in [13]. We found in our simulation Q_m better than several 1000 for all layers (for this simulation we used a Q_m of 6000 for all layers except for the Si substrate where we used $Q_m = 1000$ to account for acoustic scattering loss by the rough rear surface of the Si wafer). Velocity of sound and density of the layers were taken mainly from the literature. Dielectric loss was negligible for this resonator ($\tan\delta = 2\ 10^{-3}$ measured at 1 kHz). Series resistance R_s and inductance L_s of the electrodes were added to the resonator model as lumped elements ($R_s = 1.0\ \Omega$,

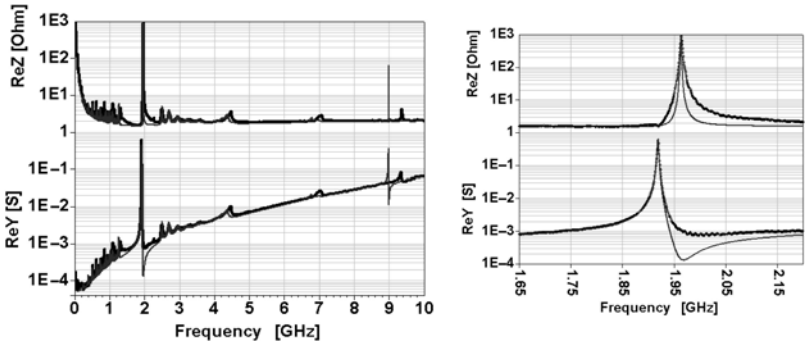

Fig. 11. Resonator at 1.95 GHz: Real part of impedance Z and admittance Y respectively. Measurement black curve, simulation blue curve. Right: anti-resonance and resonance on an enlarged scale.

$L_s = 0.061$ nH) in the circuit simulator. Additionally a resistance term proportional to $\sqrt{f}$ ($R = 1e^{-5}\sqrt{f}$) was included in the resistance. As explained above, this approximately accounts for the RF-dependent redistribution of current in the conductors, which flows closer to the edges at high frequencies. A parasitic capacitor $C_{par} = 0.19$ pF and resistor $R_{par} = 20$ kΩ to ground model the stray electric field and associated loss in the silicon substrate. Figure 11 shows that the agreement between measurement and simulation is excellent. Even the fine details of the resonator's response can be simulated and give valuable information, for example, concerning the centring of the Bragg reflector reflection band with respect to the resonator's centre frequency. The peaks in real part of the impedance (ReZ) below and above the fundamental anti-resonance peak correspond to transmission maxima of the acoustic reflector and can be used to determine the longitudinal velocity of sound in the reflector layers very accurately [13]. The small peak in the shoulder of the fundamental mode at 2.13 GHz, which is not predicted by the model, is identified as the fundamental TE mode of a parasitic resonator, which is formed between the reflector and the top electrode. Since this parasitic resonator has no bottom electrode, its resonance is at a higher frequency than that of the wanted resonator. The stray electric field excites this parasitic resonance. It can also be seen that the Bragg reflector, if well designed, suppresses higher harmonics and spurious modes very effectively. This results in a very clean resonator response and, as we will see below, in a clean filter stop-band.

The value of k_t determined from our simulation is 0.26 ($k_{eff}^2 = 6.2\%$), which is remarkably high and corresponds to the excellent orientation of the piezoelectric thin AlN film (see also Figure 7). In Figure 11 we see also that the quality factor in resonance Q_r is simulated accurately (Q_r is measured to be 1014) whereas the quality factor in anti-resonance Q_a is predicted much higher than measured (Q_a is measured to be 750). Generally we find the quality factor in resonance Q_r a bit higher than the quality factor in anti-resonance Q_a. This effect is discussed in more detail in ref. [28, 29] and can be attributed to mode conversion into modes guided by the layered structure of the SBAR. Mode conversion occurs mainly at the electrode edges of the resonator. The guided modes traveling away from the resonator can be reflected by e.g. electrode edges and give rise to the ripple seen in Figure 11. The quality factor in anti-resonance Q_a is therefore limited by mode-conversion, the quality factor in resonance Q_r by the sheet resistance of the electrodes. For an adequate description of the effects of mode conversion which give rise to additional acoustic loss and ripple a 2D or even 3D simulation is needed [28, 29].

In the following Figure 12 we show a few examples of ladder-type filters, which have been realized using high Q BAW resonators with Bragg reflector. All these filters were made on silicon substrates. As discussed above, all filters reveal a clean stop band, which is due to the additional selectivity provided by the acoustic Bragg reflector (limited bandwidth of the reflector). Higher harmonics and spurious modes are therefore very effectively suppressed. The dips in the pass-band of the filters were made intentionally by pulling the resonance frequency of the non-mass-loaded resonators and the anti-resonance frequency of the mass-loaded resonators apart. Including small series inductors at the filter ports flattens this dip. Figure 12 shows a 4-section ladder filter for 1.95 GHz, a 2-section ladder filter for 2.85 GHz, and a 3-section ladder filter for

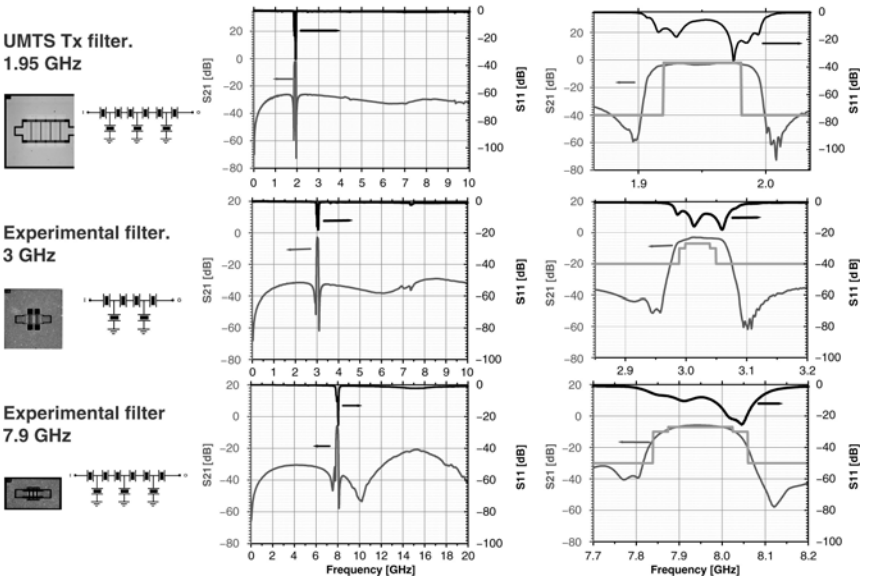

Fig. 12. 4-section, 2-section and 3-section BAW ladder-type band-pass filters for 1.95, 3, and 7.9 GHz. Left: typical layout; right: Filter curves depicting transmission S21 and reflection S11 in dB. Insertion loss is 1.9, 2.9 and 5.9 dB respectively. Bandwidth is 60 MHz, 79 MHz, and 105 MHz respectively.

8 GHz. The broad dip in the stop-band at 4.5, 6.5 and 12.5 GHz respectively is due to an LC resonance that depends on the details of the filter and package design.

In the last section we want to discuss briefly packaging of BAW filters. For BAW filters based on AlN films integration into standard CMOS processes is certainly an option, since most processing steps are compatible with standard semiconductor production. From yield and performance considerations, however, stand-alone flip chip mountable BAW filters are also attractive. As with SAW filters, there is clearly a trend to a wafer scale packages, which allows cost effective fabrication of BAW devices packaged on wafer level, which are small in area and height (Figure 13). In a System in Package (SiP) concept, which makes use of the optimal technology for each RF-function, these tiny BAW filter devices can be flip chip soldered on any carrier (e.g. on a laminate) and eventually molded into a RF front-end module [30].

6. Conclusion

Accurate BAW resonators and band-pass filters are made today in both SBAR and TFBAR technology for frequencies between 900 MHz and 12 GHz using either AlN or ZnO. In this paper we described bulk acoustic wave resonators and filters for frequencies between 2–8 GHZ on silicon wafers using c-axis oriented AlN and a Bragg acoustic interference reflector. The c-axis orientation of AlN improves with substrate temperature and with film thickness and can be influenced by the orientation

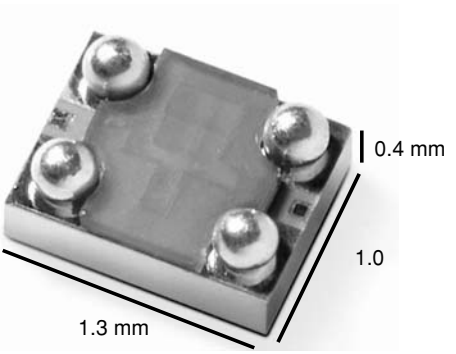

Fig. 13. Recent example of a packaged BAW filter for GSM 1900 [30].

of the underlying electrode. For Pt (111) electrodes a quasi-epitaxial relationship for the oriented growth of AlN can be found. These BAW filter devices show a remarkably high coupling coefficient k_t and a clean stop-band. The responses of the electro-acoustic resonators and filters can be described by a combination of 1-D electro-acoustic plus electromagnetic modeling. To describe acoustic losses correctly a 2-D model is required.

7. Acknowledgement

We would like to thank our colleagues R.Kiewitt, W.Brand, R.Mauczok, H.D.Bausen, H.Nulens, G.Much, D.Wiechert, at the Philips Research Laboratories in Aachen and Eindhoven. This work was partially supported by the European Commission within the Project 'Microwave Electro-Acoustic Devices for Mobile and Land based Applications (MEDCOM, IST-1999-11411)'.

References

[1] K.M. Lakin, G.R. Kline, K.T. McCarron, High Q microwave acoustic resonators and filters. IEEE Transactions on Microwave Theory a. Techniques, 41, 2139 (1993).

[2] K.M. Lakin, J. Belsick, J.F. McDonald, and K.T. McCarron, High Performance Stacked Crystal Filters for GPS and Wide Bandwidth Applications, 2001 IEEE Ultrasonics Symposium Atlanta, p. 833, 2001.

[3] R.C. Ruby, P. Bradley (SM), Y. Oshmyansky, A. Chien, Thin Film Bulk Wave Acoustic Resonators (FBAR) for Wireless Applications, 2001 IEEE Ultrasonics Symposium Atlanta, p. 833, 2001.

[4] K.M. Lakin, G.R. Kline, K.T. McCarron, Development of miniature filters for wireless applications, IEEE Transactions on Microwave Theory a. Techniques, 43, 2933 (1995).

[5] J.D. Larson III, R. Ruby, P. Bradley, Y. Oshmyansky, A BAW antenna duplexer for the 1900MHz PCS band. 1999 IEEE Ultrasonics Symposium Lake Tahoe, p. 887, 1999.

[6] K.M. Lakin, K.T. McCarron, J. Belsick, R. Rose, Filter Banks Implemented with Integrated Thin Film Resonators, 2000 IEEE Ultrasonics Symposium, Puerto Rico, p. 851, 2000.

[7] H.P. Löbl, M. Klee, R. Milsom, R. Dekker, C. Metzmacher, W. Brand, P. Lok, Materials for bulk acoustic wave (BAW) resonators and filters, Conference on Microwave Materials and their Applications MMA2000, Bled, Slovenia, September 2000, Journal of the European Ceramic Society, 21, 2633, (2001).

[8] H.P. Löbl, M. Klee, O. Wunnicke, R. Kiewitt, R. Dekker, E.v. Pelt, Piezoelectric AlN and PZT films for micro-electronic applications. 1999 IEEE Ultrasonics Symposium Lake Tahoe, p. 1031, 1999.

[9] Piezoelectric Materials for BAW Resonators and Filters, H.P.Lobl, M.Klee, C. Metzmacher, W.Brand, R. Milsom, P.Lok, F.van Straten 2001 IEEE Ultrasonics Symposium Atlanta, p. 807, 2001.

[10] H. Nowotny, E. Benes, General one-dimensional treatment of the layered piezoelectric resonator with two electrodes, J. Acoust. Soc. Am., 82, 513 (1987).

[11] H.P. Löbl, M. Klee, C. Metzmacher, W. Brand, R. Milsom, P. Lok, Piezoelectric Thin ALN Films for Bulk Acoustic Wave (BAW) Resonators, in Proceedings (SSMM) of the Asia Pacific Microwave Conference APMC 2001, Taipei, p. 37–42, 2001 and in Materials Science a. Engineering 9532, 1 (2002).

[12] J.D. Larson, P. Bradley, S. Wartenberg, R.C. Ruby, Modified Butterworth-Van Dyke Circuit for FBAR Resonators and Automated Measurement System, 2000 IEEE Ultrasonics Symposium, Puerto Rico, p. 865, 2000.

[13] R.F. Milsom, H.P. Löbl, D.N. Peligrad, J.W. Lobeek, A. Tuinhout, H.J. ten Dolle, Combined Acoustic Electromagnetic Simulation of Thin Film Bulk Acoustic Wave Filters, 2002 IEEE Ultrasonics Symposium Munich, proceedings, p. 963, 2002.

[14] H.P. Loebl, C. Metzmacher, D.N. Peligrad, R. Mauczok, M. Klee, W. Brand, R.F. Milsom, P.Lok, F.van Straten, A. Tuinhout, J.W. Lobeek, Solidly Mounted Bulk Acoustic Wave Filters for the GHz Frequency Range, 2002 IEEE Ultrasonics Symposium Munich, proceedings, p. 897, 2002.

[15] P.D. Bradley, SM, R. Ruby, A. Barfknecht, F. Geefay, C. Han, G. Gan, Y. Oshmyansky, A 5 mm $\times$ 5 mm $\times$ 1.37 mm Hermetic FBAR Duplexer for PCS Handsets with Wafer-Scale Packaging, 2002 IEEE Ultrasonics Symposium Munich, proceedings, p. 907, 2002.

[16] K.M. Lakin, Coupled Resonator Filters, 2002 IEEE Ultrasonics Symposium Munich, proceedings, p. 879, 2002.

[17] M.A. Dubois, P. Muralt, Stress and Piezoelectric properties of AlN thin films deposited onto metal electrodes by pulsed direct current reactive sputtering, J. Appl. Phys. 89, 6389 (2001).

[18] M.A. Dubois, P. Muralt, Properties of AlN thin films for piezoelectric transducers and microwave filter applications, Appl. Phys. Lett. 74, 3032 (1999).

[19] G.F. Iriarte, J. Bjurström, J. Westlinder, F. Engelmark, I.V. Katardjiev, Synthesis of c-Axis Oriented AlN Thin Films on Metal Layers: Al, Mo, Ti, TiN and Ni, 2002 IEEE Ultrasonics Symposium Munich, proceedings, p. 300, 2002.

[20] J. Kaitila, M. Yililammi, J. Molaris, J. Ellä, T. Makkonen, ZnO base thin film bulk acoustic wave filters for EGSM band, 2001 IEEE Utrasonics Symposium Atlanta, p. 803, 2001.

[21] Q.X. Su, P. Kirby, E. Komoro, M. Imura, Q. Zang, R.W. Whatmore, Thin film bulk acoustic resonators using ZnO and lead zirconium titanate thin films, IEEE Trans. MMT-49, 749 (2001).

[22] S.L. Pinkett, W.D. Hunt, B.P. Barber, P.L. Gammel, Temperature characteristics of ZnO based thin film bulk acoustic wave resonators, 2001 IEEE Utrasonics Symposium Atlanta, p. 823, 2001.

[23] K.M. Lakin, J. Belsick, J.F. McDonald, K.T: Mc Carron, Improved bulk wave resonator coupling coefficient for wide band width filters, 2001 IEEE Utrasonics Symposium Atlanta, p. 827, 2001.

[24] K.M. Lakin, J.F. McDonald, K.T: Mc Carron, Temperature compensated bulk acoustic thin film resonators, 2000 IEEE Utrasonics Symposium Puerto Rico, p. 855, 2000.
[25] M.A. Dubois, P. Muralt, V.Plesky, BAW resonators based on aluminium nitride thin films, 1999 IEEE Ultrasonics Symposium, p. 907, 1999.
[26] A. Rodriguez-Navarro, W. Otano-Rivera, J.M. Garcia-Ruiz, R. Messier & L.J. Pilione, Development of preferred orientation of polycrystalline AlN thin films deposited by rf sputtering at low temperature, J. Mater. Res., 12, 1850–1855 (1997).
[27] J.D. Larson III, R.C. Ruby, P.D. Bradley, J. Wen, S. Kok, A. Chien, Power handling and temperature coefficient studies in FBAR duplexers for the 1900 MHz PCS band, 2000 IEEE Ultrasonics Symposium Puerto Rico, proceedings, p. 869, 2000.
[28] R.F. Milsom, H.P. Loebl, C. Metzmacher, P. Lok, A. Tuinhout, F.v. Straten, 2D Model of Solidly-Mounted and Membrane BAW Devices, 2003 IEEE IEEE Utrasonics Symposium Honolulu, Hawaii, p. 1802, 2003.
[29] H.P. Loebl, R.F. Milsom, C. Metzmacher, A. Tuinhout, P. Lok, F.v. Straten, Low Level Effects in SBARS and their Application to Device Optimization, 2003 IEEE IEEE Utrasonics Symposium Honolulu, Hawaii, p. 182, 2003.
[30] H.K.J. ten Dolle, J.W. Lobeek, A. Tuinhout, J. Foekema, Balanced Lattice-Ladder Bandpass Filter in Bulk Acoustic Wave Technology, International Microwave Symposium IMS, Fort Worth, TX, paper TU5D-6, 2004.